J|A|C|S
ARTICLES
Published on Web 05/27/2006

Hydride Transfer Reaction Catalyzed by Hyperthermophilic Dihydrofolate Reductase Is Dominated by Quantum Mechanical Tunneling and Is Promoted by Both Inter- and Intramonomeric Correlated Motions

Jiayun Pang,[†] Jingzhi Pu,[‡] Jiali Gao,[‡] Donald G. Truhlar,[‡] and Rudolf K. Allemann*,[†]

Contribution from the School of Chemistry, Cardiff University, Main Building, Park Place, Cardiff, CF10 3AT, UK, and Department of Chemistry and Supercomputing Institute, University of Minnesota, 207 Pleasant Street S.E., Minneapolis, Minnesota 55455-0431

Received March 16, 2006; E-mail: allemannrk@cardiff.ac.uk

Abstract: Simulations of hydride and deuteride transfer catalyzed by dihydrofolate reductase from the hyperthermophile *Thermotoga maritima* (TmDHFR) are presented. TmDHFR was modeled with its active homodimeric quaternary structure, where each monomer has three subdomains. The potential energy function was a combined quantum mechanical and molecular mechanical potential (69 atoms were treated quantum mechanically, and 35 287, by molecular mechanics). The calculations of the rate constants by ensemble-averaged variational transition state theory with multidimensional tunneling predicted that hydride and deuteride transfer at 278 K proceeded with 81 and 80% by tunneling. These percentages decreased to 50 and 49% at 338 K. The kinetic isotope effect was dominated by contributions of bound vibrations and decreased from 3.0 to 2.2 over the temperature range. The calculated rates for hydride and deuteride transfer catalyzed by the hypothetical monomer were smaller by approximately 2 orders of magnitude. At 298 K tunneling contributed 73 and 66% to hydride and deuteride transfer in the monomer. The decreased catalytic efficiency of the monomer was therefore not the result of a decrease of the tunneling contribution but an increase in the quasi-classical activation free energy. The catalytic effect was associated in the dimer with correlated motions between domains as well as within and between subunits. The intrasubunit correlated motions were decreased in the monomer when compared to both native dimeric TmDHFR and monomeric *E. coli* enzyme. TmDHFR and its *E. coli* homologue involve similar patterns of correlated interactions that affect the free energy barrier of hydride transfer despite only 27% sequence identity and different quaternary structures.

Introduction

The ubiquitous enzyme dihydrofolate reductase (DHFR) catalyzes the conversion of 7,8-dihydrofolate (H_2F) to 5,6,7,8-tetrahydrofolate (H_4F) using reduced nicotinamide adenine dinucleotide phosphate (NADPH) as a cofactor (Figure 1). Due to the central role of the enzyme in maintaining intracellular pools of tetrahydrofolate, which acts as a one-carbon carrier during the biosynthesis of purines, thymidylate, and several amino acids, DHFR has long been recognized as a target for anticancer and antibacterial drugs. DHFRs from more than 30 organisms from the 3 domains of life have been characterized. DHFR has served as a paradigm for the study of the relationship among enzyme structure, dynamics, and catalysis of hydrogen transfer reactions (transfer of H^+, H^-, or $H^\bullet$).

Recently several experimental studies have provided strong evidence that, in addition to contributions from zero-point energies, quantum mechanical tunneling can significantly influence the rate of hydrogen transfer during many enzymatic reactions. Kinetic measurements revealed that hydrogen transfer during catalysis by DHFR from *E. coli* occurred with a strong contribution from tunneling promoted by dynamic motions of the protein.[1,2] Genomic sequence analysis combined with

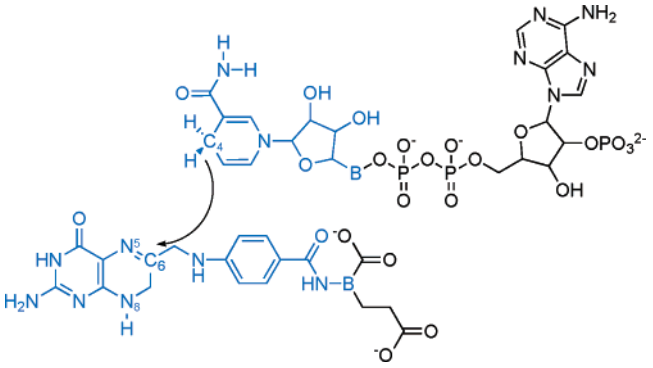

Figure 1. Schematic representation of the substrate H_2F (bottom) and the cofactor NADPH (top). The hydride and proton acceptors C6 and N5 of H_2F are labeled. Atoms treated at the QM level in the combined QM/MM potential energy surface are colored in blue, and the two boundary carbon atoms are marked "B".

[†] Cardiff School of Chemistry.
[‡] University of Minnesota.

(1) Sikorski, R. S.; Wang, L.; Markham, K. A.; Rajagopalan, P. T. R.; Benkovic, S. J.; Kohen, A. *J. Am. Chem. Soc.* **2004**, *126*, 4778−4779.

quantum mechanical and molecular dynamics simulations (QM/MM) identified an enzyme wide network of hydrogen bonds and van der Waals interactions in DHFR from *E. coli* that was suggested to influence protein dynamics and promote catalysis.[3−10] In several enzyme systems, it has been proposed that protein dynamics are coupled to tunneling, and a variety of models for active promotion of tunneling have been invoked including rate-promoting vibrations,[11−16] environmentally coupled tunneling,[17−19] vibrationally enhanced ground state tunneling,[20,21] and multidimensional tunneling.[22,23] One of the key contributors to this network of promoting motions was the surface βF-βG loop over 19 Å from the active site (Figure 2), mutations within which had previously been shown to affect the rate of hydrogen transfer. Replacement of Gly 121, a highly mobile residue located in the middle of the βF-βG loop, with Val or Leu dramatically slowed the rate of hydride transfer and weakened binding of NADPH.[24−26] Experimental and theoretical results suggested that these reductions in the rate of hydride transfer were due to significant differences in the stability of the tertiary structural elements surrounding the site of the mutation[26−28] leading to changes in the dynamic properties of the enzyme.

DHFR from the hyperthermophilic bacterium *Thermatoga maritima* (TmDHFR) is the most thermostable DHFR isolated so far. Its melting temperature of 83 °C is approximately 30 °C above the melting temperature of the *E. coli* enzyme.[29−31] Despite only 27% sequence identity between the *T. maritima* and the *E. coli* enzymes, they adopt similar tertiary structures composed of an eight-stranded mixed β-sheet (seven parallel strands, named A to G and a carboxy terminal antiparallel strand H) and of four α-helices (αB, αC, αE, and αF) (Figure 2). Like the monomeric *E. coli* enzyme, each of the two subunits of dimeric TmDHFR has three subdomains, the adenosine binding domain (ABD), the loop domain (LD), and the N-terminal domain (ND).[32,33] In contrast to all other chromosomally encoded DHFRs that have been characterized, TmDHFR forms a very stable dimer that appears to be largely responsible for its increased thermal stability.[34] Folding of TmDHFR was shown to be a two-state process between the unfolded monomers and the folded dimer; under no experimental circumstances was a folded monomer observed.[34] Interestingly, in addition to an extensive hydrophobic core in the center of the dimer interface, intersubunit hydrogen bonds between the ends of β-strands, βF and βG, confer significant stabilization on the dimer. If the mobility of the βF-βG loop is also important in TmDHFR catalysis as had been suggested for the *E. coli* enzyme, these interactions might also influence the rate of hydrogen transfer in TmDHFR.

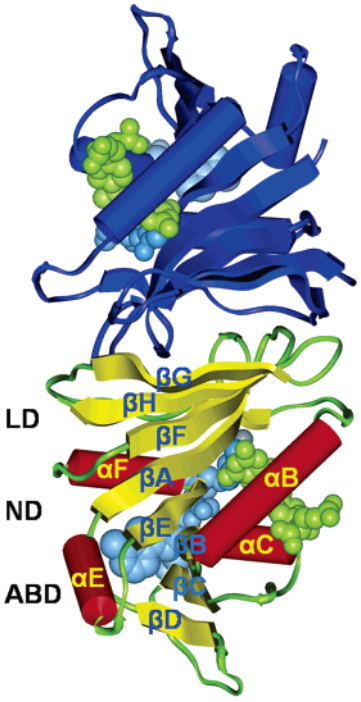

Figure 2. Structure of TmDHFR (1D1G.pdb).[32] The elements of secondary structure of subunit A are labeled, and α-helices, β-strands, and loop regions are colored red, yellow, and green, respectively. Subunit B is colored in blue. H_2F and NADPH are represented as space-filling models.

Pre-steady-state studies of TmDHFR catalysis indicated a biphasic temperature dependence of the kinetic isotope effect (KIE) for H- and D-transfer.[30] Below 25 °C, the KIEs depended on the temperature. The ratio of the preexponential factors for H- and D- transfer was strongly inverse suggesting a substantial contribution from quantum mechanical tunneling to the reaction. For higher temperatures, the only weakly temperature dependent KIEs were consistent with an environmentally coupled model for tunneling.[17] Similarly, the experimentally observed weak temperature dependence of the KIEs in DHFR from *E. coli* has been interpreted in terms of both the environmentally coupled

(2) Swanwick, R. S.; Maglia, G.; Tey, L. H.; Allemann, R. K. *Biochem. J.* **2006**, *394*, 259−265.
(3) Agarwal, P. K.; Billeter, S. R.; Rajagopalan, P. T. R.; Benkovic, S. J.; Hammes-Schiffer, S. *Proc. Natl. Acad. Sci. U.S.A.* **2002**, *99*, 2794−2799.
(4) Watney, J. B.; Agarwal, P. K.; Hammes-Schiffer, S. *J. Am. Chem. Soc.* **2003**, *125*, 3745−3750.
(5) Wong, K. F.; Watney, J. B.; Hammes-Schiffer, S. *J. Phys. Chem. B* **2004**, *108*, 12231−12241.
(6) Wong, K. F.; Selzer, T.; Benkovic, S. J.; Hammes-Schiffer, S. *Proc. Natl. Acad. Sci. U.S.A.* **2005**, *102*, 6807−6812.
(7) Radkiewicz, J. L.; Brooks, C. L. *J. Am. Chem. Soc.* **2000**, *122*, 225−231.
(8) Rod, T. H.; Radkiewicz, J. L.; Brooks, C. L. *Proc. Natl. Acad. Sci. U.S.A.* **2003**, *100*, 6980−6985.
(9) Thorpe, I. F.; Brooks, C. L. *J. Phys. Chem. B* **2003**, *107*, 14042−14051.
(10) Schnell, J. R.; Dyson, H. J.; Wright, P. E. *Annu. Rev. Biophys. Biomol. Struct.* **2004**, *33*, 119−140.
(11) Antoniou, D.; Caratzoulas, S.; Kalyanaraman, C.; Mincer, J. S.; Schwartz, S. D. *Eur. J. Biochem.* **2002**, *269*, 3103−3112.
(12) Mincer, J. S.; Schwartz, S. D. *J. Proteome Res.* **2003**, *2*, 437−439.
(13) Mincer, J. S.; Schwartz, S. D. *J. Phys. Chem. B* **2003**, *107*, 366−371.
(14) Mincer, J. S.; Schwartz, S. D. *J. Chem. Phys.* **2004**, *120*, 7755−7760.
(15) Basner, J. E.; Schwartz, S. D. *J. Phys. Chem. B* **2004**, *108*, 444−451.
(16) Antoniou, D.; Schwartz, S. D. *Proton transfer in condensed phases: beyond the Kramers paradigm*. Kluwer: Dordrecht, 2000.
(17) Knapp, M. J.; Klinman, J. P. *Eur. J. Biochem.* **2002**, *269*, 3113−3121.
(18) Knapp, M. J.; Rickert, K.; Klinman, J. P. *J. Am. Chem. Soc.* **2002**, *124*, 3865−3874.
(19) Kohen, A. *Progress in Reaction Kinetics and Mechanism* **2003**, *28*, 119−156.
(20) Sutcliffe, M. J.; Scrutton, N. S. *Eur. J. Biochem.* **2002**, *269*, 3096−3102.
(21) Masgrau, L.; Basran, J.; Hothi, P.; Sutcliffe, M. J.; Scrutton, N. S. *Arch. Biochem. Biophys.* **2004**, *428*, 41−51.
(22) Garcia-Viloca, M.; Truhlar, D. G.; Gao, J. *Biochemistry* **2003**, *42*, 13558−13575.
(23) Truhlar, D. G. *Variational transition state theory and multidimensional tunneling for simple and complex reactions in the gas phase, solids, liquids and enzymes*. CRC/Taylor and Francis: Boca Raton, FL, 2006.
(24) Cameron, C. E.; Benkovic, S. J. *Biochemistry* **1997**, *36*, 15792−15800.
(25) Rajagopalan, P. T. R.; Lutz, S.; Benkovic, S. J. *Biochemistry* **2002**, *41*, 12618−12628.
(26) Swanwick, R. S.; Shrimpton, P. J.; Allemann, R. K. *Biochemistry* **2004**, *43*, 4119−4127.
(27) Thorpe, I. F.; Brooks, C. L. *Proteins* **2004**, *57*, 444−457.
(28) Thorpe, I. F.; Brooks, C. L. *J. Am. Chem. Soc.* **2005**, *127*, 12997−13006.
(29) Maglia, G. *The importance of molecular dynamics in dihydrofolate reductase catalysis*. University of Birmingham: 2004.
(30) Maglia, G.; Allemann, R. K. *J. Am. Chem. Soc.* **2003**, *125*, 13372−13373.
(31) Maglia, G.; Javed, M. H.; Allemann, R. K. *Biochem. J.* **2003**, *374*, 529−535.
(32) Dams, T.; Auerbach, G.; Bader, G.; Jacob, U.; Ploom, T.; Huber, R.; Jaenicke, R. *J. Mol. Biol.* **2000**, *297*, 659−672.
(33) Sawaya, M. R.; Kraut, J. *Biochemistry* **1997**, *36*, 586−603.
(34) Dams, T.; Jaenicke, R. *Biochemistry* **1999**, *38*, 9169−9178.

tunneling model[1] and multidimensional tunneling modulated by variational transition state effects on the location and free energy requirement of the dynamical bottleneck.[35] We note that the multidimensional tunneling approximation used before[35] and in this paper includes tunneling paths with a temperature-dependent distribution of the donor−acceptor distances.[23,36,37]

Here we report combined quantum mechanical and molecular mechanical (QM/MM) calculations[38−40] to determine the rates of the hydride transfer reaction catalyzed by TmDHFR as a function of temperature using ensemble-averaged variational transition state theory with multidimensional tunneling (EA-VTST/MT). The QM/MM potential energy function employed the same parameters as those used previously[22] for DHFR from *E. coli*. The behavior of the native TmDHFR dimer was compared to that of the experimentally inaccessible TmDHFR monomer. The results suggest that quantum mechanical tunneling makes a significant contribution to the reaction rate at all temperatures and that dimerization is not only important for the thermal stability of TmDHFR but also for its catalytic activity.

Results and Discussion

Potential of Mean Force for TmDHFR Catalysis. The first stage in the calculation of the rate constants for hydride transfer from NADPH to dihydrofolate was to compute the single-reaction-coordinate quasi-classical free energy of activation, which can be obtained by adding quantization effects to the classical mechanical potential of mean force (CM-PMF) as a function of the reaction coordinate z.[39,41] It is generally assumed that protonation of N5 of H_2F precedes hydride transfer from NADPH to C6 of H_2F.[22,42] The substrate was therefore protonated on N5 for all computational studies. Figure 3 displays the computed CM-PMF along the hydride transfer reaction coordinate for 5, 25, and 65 °C. These curves were obtained using the WHAM method.[43,44] Figure 3 shows that when the temperature is increased from 5 to 25 °C both the transition state and the product state are destabilized relative to the reactants. Such an increase of the classical free energy barrier has also been observed for DHFR from *E. coli*.[35] At 65 °C however, both states are stabilized. Although the reaction is endergonic, the transition states (as judged by the negative value of z^* and by their occurring slightly prior to the minimum in the quantized vibrational correction) are slightly early, which is counter to expectations based on the Hammond postulate.[45] The position of the transition state is initially shifted toward the product state when the temperature was increased from 5 to 25 °C, but at 65 °C the transition state is more reactant-like.

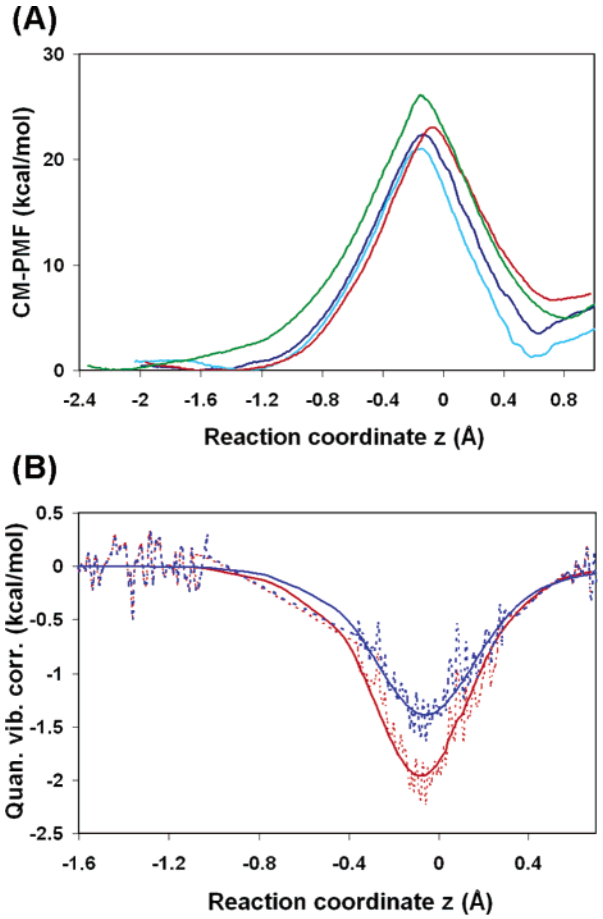

Figure 3. (A) The computed classical mechanical PMF obtained by simulations of dimeric TmDHFR at 278 K (blue line), 298 K (orange line), and 338 K (light blue line). The green line represents the classical mechanical PMF of monomeric TmDHFR for the simulation at 298 K. (B) The quantized vibrational energy corrections to the classical free energies of activation. The data of H-transfer are shown in red dots, and the data of D-transfer are shown in blue dots. These initial data were fit to Eckart functions to obtain the curves shown in red and blue for H and D, respectively.

Table 1. Computed Free Energy of Activation in kcal/mol for H- and D-Transfer at Three Temperatures[a]

	dimer 5 °C		dimer 25 °C		dimer 65 °C		monomer 25 °C	
	H	D	H	D	H	D	H	D
classical	22.2	22.2	22.9	22.9	20.9	20.9	25.5	25.5
+ quan. vib.	19.9	20.4	20.7	21.2	19.0	19.4	24.2	24.6
+ recrossing	20.1	20.7	20.9	21.5	19.1	19.6	24.2	24.7
+ tunneling	19.2	19.8	20.1	20.7	18.6	19.1	23.5	23.9

[a] The first row is the classical free energy of activation; the second row is the free energy of activation after adding the quantized nuclear vibrational corrections; the third row is the value after including the effects of barrier recrossing; and the fourth row is the final phenomenological free energy of activation after including the effects of tunneling.

The classical free energy barrier at 65 °C is narrower than those at the lower temperatures.

The computed classical free energies of activation, which include the loss of the free energy $G^{CM}_{R,F}$ of the reactive normal mode of the reactant,[41] are 22.2, 22.9, and 20.9 kcal/mol for 5, 25, and 65 °C (Table 1). The value of $G^{CM}_{R,F}$ is 0.65 kcal/mol at 5 °C, 0.50 kcal/mol at 25 °C, and 0.45 kcal/mol at 65 °C for both H- and D-transfer. The previously reported classical free energies of DHFR from *E. coli* were 14.5 and 16.1 kcal/mol for 5 and 25 °C,[22,35] significantly lower than the values

(35) Pu, J.; Ma, S.; Gao, J.; Truhlar, D. G. *J. Phys. Chem. B* **2005**, *109*, 8551−8556.
(36) Garrett, B. C.; Truhlar, D. G. In *Physical and Chemical Aspects of Hydrogen Transfer*; Hynes, J. T., Limbach, H. H., Eds.; Vol. 1 of Handbook of Hydrogen Transfer; Wiley-VCH: Weinheim, Germany, 2006 (in press).
(37) Garrett, B. C.; Truhlar, D. G.; Wagner, A. F.; Dunning, T. H. *J. Chem. Phys.* **1983**, *78*, 4400−4413.
(38) Gao, J.; Amara, P.; Alhambra, C.; Field, M. J. *J. Phys. Chem. A* **1998**, *102*, 4714−4721.
(39) Gao, J.; Truhlar, D. G. *Annu. Rev. Phys. Chem.* **2002**, *53*, 467−505.
(40) Gao, J. *Rev. Comput. Chem.* **1995**, *7*, 119−185.
(41) Garcia-Viloca, M.; Alhambra, C.; Truhlar, D. G.; Gao, J. *J. Chem. Phys.* **2001**, *114*, 9953−9958.
(42) Cummins, P. L.; Gready, J. E. *J. Am. Chem. Soc.* **2001**, *123*, 3418−3428.
(43) Kumar, S.; Bouzida, D.; Swendsen, R. H.; Kollman, P. A.; Rosenberg, J. M. *J. Comput. Chem.* **1992**, *13*, 1011−1021.
(44) Rajamani, R.; Naidoo, K. J.; Gao, J. *J. Comput. Chem.* **2003**, *24*, 1775−1781.
(45) Hammond, G. S. *J. Am. Chem. Soc.* **1953**, *77*, 334−338.

Table 2. Locations of the Transition State (z^*) Identified from the Classical Mechanical Potential of Mean Force (CM-PMF) Calculations; the Average Values of Three Internuclear Distances Involving the Hydride (H), Donor (C4), and Acceptor (C6); and the Average Angle among the Donor, the Transferred Hydride, and the Acceptor in the Configurations with $z^* \pm 0.1$ Å near the Transition State[a]

	z^*	C6–H	C4–H	C6–C4	C6–H–C4
dimer 5 °C	−0.135	1.47 (0.04)	1.28 (0.03)	2.70 (0.06)	157 (7)
dimer 25 °C	−0.075	1.40 (0.04)	1.33 (0.04)	2.70 (0.06)	164 (7)
dimer 65 °C	−0.145	1.44 (0.05)	1.31 (0.04)	2.69 (0.06)	160 (8)
monomer 25 °C	−0.155	1.48 (0.04)	1.28 (0.03)	2.73 (0.06)	161 (7)

[a] The unit of distance is Å, and the unit of angle is degree. The standard deviation is in parentheses.

calculated here for TmDHFR. The rates calculated here for TmDHFR catalysis are lower than those determined experimentally,[30] while the corresponding Arrhenius activation energies are higher (computing these activation energies in kcal/mol from the rate constants at 5 and 65 °C, we obtain 12.8 (experiment for H), 13.4 (experiment for D), 22.5 (theory for H), and 23.6 (theory for D)). The computational results agree with experiment in that hydride transfer catalyzed by TmDHFR is significantly slower than that in the *E. coli* enzyme at all experimentally accessible temperatures.[29−31,46]

The inclusion of contributions from the quantized vibrational energies lowers the free energy of activation by 1.9−2.2 kcal/mol for H-transfer and by 1.5−1.7 kcal/mol for D-transfer (Table 1 and Figure 3). The extent of this correction is similar to that reported previously for the hydride transfer reactions in DHFR from *E. coli*.[22,35,47] The transition state for the TmDHFR catalyzed reaction depends slightly on the temperature; its location (z^*) varies from −0.135 Å at 5 °C to −0.075 Å at 25 °C and −0.145 Å at 65 °C, suggesting a nonmonotonic isotopic difference in the vibrational energy as a function of temperature. The average distance between the donor and acceptor carbons at z^* varies only slightly; in particular it changes from 2.70 to 2.69 Å from 5 and 65 °C, while the average C4−H−C6 angle changes from 157° to 160°. The average values of the breaking and forming bond distances vary nonmonotonically with temperature as shown in the first three rows of Table 2.

Quantum Mechanical Tunneling and Rate Constants. To obtain rate constants for hydrogen transfer during TmDHFR catalysis, transmission coefficients accounting for multidimensional tunneling (κ) and dynamical recrossing (Γ) were determined and expressed in the overall ensemble-averaged transmission coefficient (γ) (Table 3). It is important to emphasize here that the standard deviations in Table 3 (and the other tables) presented here are not error bars. They are standard deviations of the distribution corresponding to the transition state ensemble; this is a real effect of the fluctuating protein environment (which causes fluctuations in the barrier widths, overbarrier reaction paths, and tunneling paths), not an error. The transmission coefficient is clearly dependent on the temperature and contributes approximately twice as much to the overall reaction rate at 5 °C than at 65 °C. The temperature dependence of γ is a consequence of a strongly temperature dependent contribution from tunneling, while dynamical recrossing was temperature independent. At the higher temperatures, classical over-the-barrier transfers clearly compete more efficiently with quantum mechanical tunneling than at lower temperatures; i.e., the effect of the Boltzmann factors (which enable tunneling to compete more effectively with over-the-barrier processes as the temperature is lowered) contribute more to the increased hydrogen transfer rates than does the temperature-dependent barrier narrowing. It is important to stress that tunneling probabilities are sensitive to the protein geometry, and at the extremes of the distribution of geometries in the transition state ensemble, there can be large variations in the competition between overbarrier processes and tunneling. The inclusion of tunneling and dynamical recrossing lowers the overall free energy of activation for H- and D-transfer by 0.7 and 0.6 kcal/mol at 5 °C and by 0.4 and 0.3 kcal/mol at 65 °C.

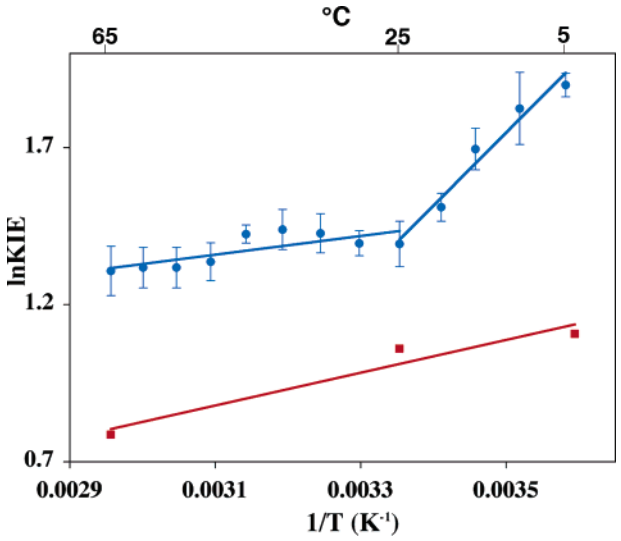

Figure 4. Comparison of the temperature dependence of ln KIE obtained from the final computed rate constants $k^{EA-VTST/MT}$ for H- and D-transfer obtained in this study (red) and from the experimentally determined rates for H- and D-transfer (blue)[30] during catalysis by TmDHFR.

The final computed rate constants $k^{EA-VTST/MT}$, which are the product of the rate constants obtained from the stage-1 quasi-thermodynamic free energy of activation $\Delta G^{(1)}_{act}$ (given in the second row of Table 1) and the average transmission coefficient γ, are shown in Table 4 and Figure 4. The quasi-classical rate constants k^{QC}, which neglect contributions from the tunneling factor κ, are also shown in Table 4. Comparing k^{QC} with $k^{EA-VTST/MT}$ gives an indication of the degree of tunneling which ranges from ∼80% at 5 °C to ∼50% at 65 °C (as explained in the methods section, these are underestimates). The TmDHFR-catalyzed hydrogen transfer reaction therefore proceeds predominantly by way of quantum mechanical tunneling as had been proposed earlier from experimental results.[30]

The temperature dependence of the computationally derived kinetic isotope effects was used to determine the parameters of the Arrhenius equation:

$$\ln(\mathrm{KIE}) = -\frac{\Delta E_a}{R}\frac{1}{T} + \ln\left(\frac{A_H}{A_D}\right)$$

where A_H/A_D is the KIE at infinite temperature, and ΔE_a, the difference in the activation energies for H- and D-transfer. The calculated ratio of A_H/A_D is 0.47, which is below the experimental value of 1.56 ± 0.47 for temperatures above 25 °C. The

(46) Fierke, C. A.; Johnson, K. A.; Benkovic, S. J. *Biochemistry* **1987**, *26*, 4085−4092.
(47) Agarwal, P. K.; Billeter, S. R.; Hammes-Schiffer, S. *J. Phys. Chem. B* **2002**, *106*, 3283−3293.

Table 3. Overall Ensemble-Averaged Transmission Coefficient (γ) and the Transmission Coefficient Components Due to Recrossing (Γ) and Tunneling (κ)[a]

	dimer 5 °C		dimer 25 °C		dimer 65 °C		monomer 25 °C	
	H	D	H	D	H	D	H	D
κ	5.25 (1.38)	4.92 (0.89)	4.13 (0.99)	3.81 (0.54)	2.00 (0.38)	1.97 (0.52)	4.05 (1.86)	3.61 (1.37)
Γ	0.66 (0.29)	0.63 (0.28)	0.66 (0.28)	0.64 (0.28)	0.79 (0.21)	0.71 (0.26)	0.90 (0.13)	0.87 (0.21)
γ	3.38 (1.74)	3.09 (1.55)	2.72 (1.31)	2.44 (1.12)	1.64 (0.66)	1.51 (0.86)	3.69 (1.74)	2.98 (1.12)

[a] The standard deviation is in parentheses.

Table 4. Reaction Rate Constants and the Kinetic Isotope Effects (KIEs)

		H	D	KIE
dimer 5 °C	k^{QC}	0.00084	0.00028	2.90
	$k^{EA-VTST/MT}$	0.0043	0.0014	3.02
	k^{exp} [a]	0.044	0.0066	6.67
dimer 25 °C	k^{QC}	0.0026	0.0010	2.58
	$k^{EA-VTST/MT}$	0.011	0.0037	2.88
	k^{exp} [a]	0.16	0.042	4.02
dimer 65 °C	k^{QC}	2.8	1.2	2.25
	$k^{EA-VTST/MT}$	5.9	2.7	2.19
	k^{exp} [a]	2.1	0.57	3.36
monomer 25 °C	k^{QC}	9.6×10^{-6}	4.5×10^{-6}	2.11
	$k^{EA-VTST/MT}$	3.9×10^{-5}	1.5×10^{-5}	2.52

[a] Data for k^{exp} from ref 30.

computed ΔE_a of -1.04 kcal/mol compares well with the experimental value of -0.60 ± 0.25 kcal/mol determined for the range above 25 °C. Interestingly, the biphasic behavior of the KIE observed experimentally, where the KIEs were temperature independent above 25 °C but changed with temperature below, was not reproduced computationally. This may be indicative of a conformational change of TmDHFR at 25 °C. With currently accessible time scales, molecular modeling would not normally be expected to detect such a change in the reactive conformation. Another possibility is that the break is related to the nonmonotonic temperature dependence of the C6−H bond distance at the dynamical bottleneck. It has sometimes been argued that thermophilic enzymes have evolved to enhance tunneling at the high temperatures at which they naturally operate, such that tunneling may be relatively more important at high temperature.[48] In the present case, we see that even though the high-temperature reaction is dominated by tunneling, an even larger percentage of reaction proceeds by tunneling at lower temperature, which is the expected result[36] based on experience with gas-phase reactions.

Tunneling and Rate Constants for Catalysis by TmDHFR Monomer. The dimeric structure of TmDHFR is very stable, and no folded monomer was detected in chemically induced unfolding experiments.[34] The unfolding equilibrium strictly followed a two-state model between the folded dimer and the unfolded monomer. The thermal melting transition occurred above 80 °C,[31] and the quaternary structure of TmDHFR was identified as the principal source of its high stability.[32,34] We have constructed a computational model of the monomer of TmDHFR by deleting the coordinates of one of the symmetry related subunits, and we have computed the rate constants for hydrogen transfer catalyzed by the hypothetical monomer at 25 °C. The structure of the monomer stayed intact during the time course of the 1.2 ns simulations (RMSD < 3 Å). In an independent 10 ns molecular dynamics simulation at 25 °C using a molecular mechanics force field, a maximum RMSD of 2.7 Å for all the backbone atoms was determined (see Supporting Information). Compared to the native dimer, the transition state of the free energy barrier height along the CM-PMF was destabilized by 2.6 kcal/mol, and the classical free energy barrier was significantly wider (Figure 3). When the quantized vibrational energy requirements were taken into account, the difference in the free energy of activation of the monomer and the native dimer increased to 3.5 and 3.4 kcal/mol for H- and D-transfer, respectively. The rate constants $k^{EA-VTST/MT}$, which take the transmission coefficient into account, were reduced by more than 2 orders of magnitude relative to the values for the dimer (Table 4) suggesting that the hypothetical monomer of TmDHFR would be kinetically compromised.

A comparison of the quasi-classical rate constants k^{QC} with $k^{EA-VTST/MT}$ revealed that the degree of tunneling is 75 and 70% for H- and D-transfer at 25 °C, which is similar to the 76 and 73% observed for the TmDHFR dimer at the same temperature. The inclusion of tunneling and dynamical recrossing into the calculations for the monomer lowered the free energy of activation by 0.7 and 0.8 kcal/mol for H- and D-transfer, respectively. These reductions were again similar to those observed for dimeric TmDHFR. While the donor−acceptor distance between C4 of NADPH and C6 of H_2F differed by only 0.03 Å between the dimer and the monomer (Table 2), the location of the transition state (z^*) varied significantly. The transition state in the monomer was much more reactant-like ($z^* = -0.155$ Å) compared to the native dimer ($z^* = -0.075$ Å).

These results suggest that dimerization not only increases the thermodynamic stability of TmDHFR[34] but also increases its catalytic activity with respect to hydrogen transfer largely through altering the barrier of the classical PMF. Passing from the active dimeric form to the catalytically less active monomer actually raises the tunneling transmission coefficient, not lowers it. Thus although tunneling dominates the catalyzed reaction, it can be said to anticatalyze the reaction (decreased catalysis in the active catalyst as compared to the monomer), which disagrees with the hypothesis[48] that enzymes have been evolutionarily optimized to enhance tunneling. In fact the trend is the expected one since it has been argued that[49] "proteins may have evolved to increase the rate of hydrogen-atom transfer by creating a lower, wider barrier. Such a barrier would actually decrease the amount of tunneling in the enzyme reaction." Similarly, one expects that deactivating a protein raises the effective barrier, usually making it thinner, and usually increasing the fraction of reaction that occurs via tunneling. We note that Hwang and Warshel[50] concluded that quantum mechanical effects can make a non-negligible contribution to catalysis, but

(48) Kohen, A.; Cannio, R.; Bartolucci, S.; Klinman, J. P. *Nature* **1999**, *399*, 496−499.

(49) Kemsley, J. *Chemical and Engineering News* **2003**, *81* (Sept. 22), 29−30.

Table 5. Selected Atomic Distances between the Substrate H_2F, Cofactor NADPH, and the Active Site Residue Arg28 in the Reactant Michaelis Complex State (RS), Transition State (TS), and Product State (PS)[a]

atom labels		TmDHFR dimer			TmDHFR monomer		
		RS	TS	PS	RS	TS	PS
H_2F N5	NADPH O7N	3.71 (0.69)	3.16 (0.30)	3.36 (0.27)	3.85 (0.39)	3.79 (0.28)	5.09 (0.36)
H_2F N8	NADPH O7N	4.42 (0.58)	5.12 (0.35)	5.88 (0.23)	3.43 (0.32)	3.17 (0.28)	4.14 (0.33)
Arg28 NH1	NADPH O7N	5.69 (0.35)	3.24 (0.62)	3.32 (0.35)	7.87 (0.52)	7.91 (0.50)	8.50 (0.74)

[a] The results from 25 °C simulations of the TmDHFR dimer and monomer. The standard deviations are shown in bracket. See Figure 5 for the atom labels.

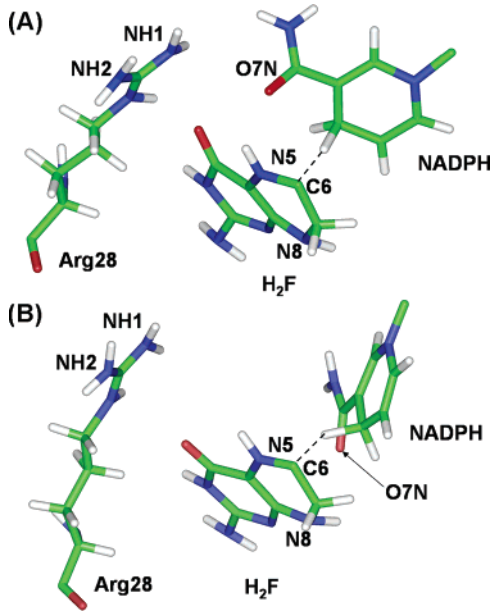

Figure 5. Snapshots of transition state configurations of H_2F and NADPH in the active sites of (A) the dimer and (B) the hypothetical monomer of TmDHFR. For clarity, only the pterin ring of H_2F and the nicotinamide ring of NADPH are shown.

their method does not sort out the separate contributions of quantized vibrations and tunneling. In later work, Olsson and co-workers[51] concluded that nuclear quantum mechanical effects are similar in enzymes and in reference reactions in solution.

We have examined the hydrogen bonding patterns in the active sites of the dimeric and monomeric TmDHFR systems. It is found that there are noticeable differences in the orientation of the nicotinamide ring of the NADPH cofactor (Figure 5). Arg28 in TmDHFR, which replaces Leu28 in DHFR from *E. coli*, donates a hydrogen bond to the nicotinamide oxygen, and this interaction plays a strong stabilizing role in the reaction. In the dimer, the magnitude of its stabilization effect (computed by the method of Cui and Karplus[52] as in ref 22) is 14 kcal/mol at the transition state and 8 kcal/mol in the product state (both values are relative to the reactant Michaelis state). The corresponding average heavy atom distance is 3.24 Å at the transition state and 5.69 Å for the Michaelis complex at 25 °C (Table 5). However, such a hydrogen bond was not formed between the side chain nitrogen (NH1) of Arg28 and O7N of NADPH in the monomer where the distance between the two atoms is approximately 8 Å (Table 5), and the stabilization effect of Arg28 is reduced to 4 kcal/mol at the transition state (vs 14 kcal/mol in the dimer). It is interesting to note that the two conformational orientations of the nicotinamide have also been observed in our previous study of DHFR from *E. coli*.[22] These conformations are largely determined by interactions of the O7N atom with one or the other of the hydrogen atoms attached to the pteridine N5 or N8 atoms. In DHFR from *E. coli*, it was found that the interaction with the N5 orientation is enhanced at the transition state and product state, whereas the N8 site is preferred in the Michaelis complex state. Apparently to compensate for larger thermal fluctuations at higher temperatures, the hyperthermophilic enzyme has Leu28 replaced by Arg28 to further assist the nicotinamide ring in adopting the N5 orientation, which is preferred for transition state stabilization. On the other hand, in the monomeric TmDHFR, Arg28 has moved away from the nicotinamide binding pocket. Thus, we suggest that the replacement of Leu28 by Arg28 in TmDHFR has the consequence of enforcing the cofactor to adopt a conformation with favorable transition state stabilization, and this is necessary to avoid larger dynamic fluctuations at the higher temperatures where TmDHFR functions.

Analysis of Correlated Motions. To examine how changes in the quaternary structure of TmDHFR might affect the apparent reaction rates for hydrogen transfer, the trajectories of the molecular dynamics simulations of the native dimer and the hypothetical monomer were analyzed for the presence of residues that are dynamically coupled to each other. Molecular dynamics simulations of *E. coli* DHFR had previously revealed correlations between the movements of several elements of secondary structure.[5,6,8,22,28] In that enzyme the catalytically important M20 and βF-βG loops showed particularly strong correlations,[8] which may be associated with either correlated motions or correlated interactions (we will use the former term). These motions were reduced in catalytically compromised βF-βG loop mutants[8] suggesting a link between correlated motions and catalytic activity. Since βF and βG and the connecting βF-βG loop are part of the dimer interface in TmDHFR, the correlated motions between the βF-βG and M20 loops might be impaired leading to a reduction of the rate of hydrogen transfer. We have therefore employed covariance analysis across the trajectories of the hydrogen transfer simulations of TmDHFR for the progression from reactants to products. The resulting matrices (Figure 6) represent the correlation coefficients of the spatial fluctuations between the Cα atoms of amino acid residue pairs and describe the correlated motions within individual subunits and between the subunits in the dimer.

Inspection of the covariance matrix for the TmDHFR dimer indicated significant amounts of positively correlated motions between the loop domains from individual subunits as would be expected from the structure of TmDHFR. Particularly strong positive correlations were observed across the subunit boundaries between βF and βG and the connecting βF-βG loop. Interestingly, positive correlations were also observed between

(50) Hwang, J. K.; Warshel, A. *J. Am. Chem. Soc.* **1996**, *118*, 11745−11751.
(51) Olsson, M. H. M.; Siegbahn, P. E. M.; Warshel, A. *J. Am. Chem. Soc.* **2004**, *126*, 2820−2828.
(52) Cui, Q.; Karplus, M. *J. Am. Chem. Soc.* **2001**, *123*, 2284−2290.

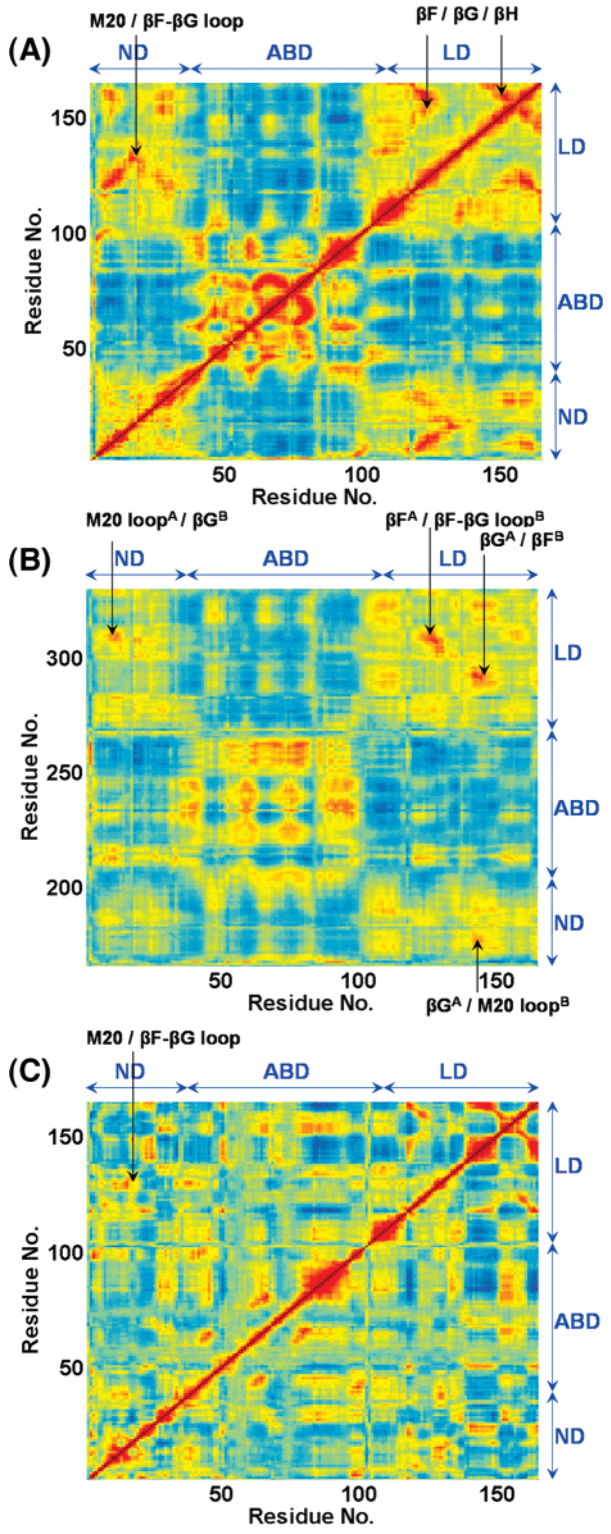

Figure 6. Matrices of correlated motions of the Cα atoms within subunit A in dimeric TmDHFR (A), between subunit A and subunit B (B), and in monomeric TmDHFR (C). These matrices were generated using trajectories of the simulations at 298 K. The color scale ranges from blue for perfect negative correlation to red for perfect positive correlation. The matrixes are labeled according to the domain divisions of TmDHFR.

individual adenosine binding domains; this indicated that the correlated motions in the loop domains are linked to motions of the distal ABD.

Analysis of the covariance matrices for dimer and monomer indicated that the extent of coupled motions is decreased in the monomer relative to the individual subunits of the native dimer. The positive correlations in the subunits of the dimer were mostly found within the domains of the subunits, while interdomain movements were characterized by negative correlations (Figure 6). In the subunits of the dimer several areas of strong positive correlation were identified, namely between helix αF and the βF-βG loop, between βF and βG, as well as between the βG-βF and M20 loops. The interactions between residues 14−17 of the M20 loop and residues 131−133 of the βF-βG loop were observed both in the dimer and the monomer but were more pronounced in the dimer. In particular, the short hydrogen bond between the backbone nitrogen of Ile15 in the M20 loop and the carbonyl oxygen of Ile131 of the βF-βG loop was maintained during the full length of the simulation process (data not shown) suggesting that the interaction between these two loops is involved in maintaining the structure of the dimer. Interestingly, while the correlated motions within TmDHFR did qualitatively not change with increasing temperature, their intensity was reduced (see Supporting Information). This result suggests that the correlated motions remain largely unaltered even at higher temperatures where increased random thermal fluctuations would be expected.

While several of the strong intra-subunit correlated motions identified in the TmDHFR dimer are also present in the monomer, their intensity is reduced. This agrees with the proposals[11−15,17,20,22] that the dynamic properties of DHFR are coupled to catalysis for instance through promoting vibrational modes where a local structural change can have a global impact through the perturbation of the normal modes. DHFRs from *E. coli* and *T. maritima* may have evolved with their different quaternary structures in a way that optimizes the coupling of protein motions with the reaction coordinate as is suggested by the observation that the catalytically less active monomer of TmDHFR was characterized by a reduction of the coupled motions when compared to both the TmDHFR dimer and the naturally monomeric enzyme from *E. coli*.

The results presented here show that hydride transfer in TmDHFR occurs with a substantial contribution from quantum mechanical tunneling (>50%) at all temperatures examined. In the experimentally unobservable TmDHFR monomer, the tunneling contributions to the reaction are similar to that found in the dimer, but the overall activation energy is increased suggesting that the hypothetical monomer would be kinetically compromised. Dimerization may therefore not only be important for stability but also for the catalytic efficiency of the hyperthermophilic DHFR from *T. maritima*. Covariance analysis indicates that the two subunits of TmDHFR move in a correlated fashion. Within individual subunits of TmDHFR, several of the correlated motions that had been identified previously in DHFR from *E. coli*, such as the concerted movement of the M20 and the βF-βG loops, were also present. Homologous proteins may therefore use similar patterns of correlated motions to facilitate hydrogen transfer even when their amino acid sequences and their quaternary structures are different.

Methods

Model of the Enzyme−Substrate−Coenzyme Complex. The published crystal structure (1D1G.pdb) of dimeric TmDHFR with the inhibitor methotrexate (MTX) and the reduced cofactor (NADPH) was used to build the model for the present study.[32] The structure of 7,8-dihydrofolate was superimposed onto MTX. The pterin ring of 7,8-

dihydrofolate was rotated by approximately 180° so that orientation and position of the substrate were similar to those seen in the crystal structures of the enzyme with folate-like substrates in the active site. The coordinates for MTX were then deleted. Key interactions involving ligand binding were monitored during the simulations as a validation for the model. Asp27 was assumed to be deprotonated at neutral pH in agreement with previous work,[53] while the protonation states of all other ionizable groups were set for pH 7. N5 of the substrate was protonated as in previous studies.[22,42] The final protein structure was solvated with a previously equilibrated rectangular box of water molecules with the initial dimensions of 100 Å × 60 Å × 60 Å. The resulting system was neutralized by placing four Na^+-ions near negatively charged residues at distances greater than 17 Å from the active sites. The total number of atoms resulting from this process is 35 356. To study the effect of dimerization, a separate series of calculation was carried out on the monomer structure of TmDHFR, which was obtained by deleting one subunit from the dimeric structure. The two subunits are related by a two-fold axis of symmetry and show a root-mean-square deviation smaller than 0.21 Å. The monomer was then solvated in a water box with dimensions 60 Å × 60 Å × 60 Å and neutralized with two Na^+ ions.

Computational Methodology. A combined QM/MM approach was used for the simulation of the TmDHFR system. 69 atoms (39 atoms from 5-protonated 7,8-H_2F and 30 atoms from NADPH) in one active site (subunit A) were treated at the QM level, while the rest of the system was treated at the MM level. The two boundary atoms were treated by the generalized boundary orbital (GHO) method (Figure 1).[38] A simple valence bond term was added with the same parameters as those used for DHFR from *E. coli*. The CHARMM27 force field was used to present the protein and TIP3P model for water similarly to a previous study of the hydride transfer catalyzed by DHFR from *E. coli*.[22] All calculations employed periodic boundary conditions.

The rates for hydride and deuteride transfer were calculated for the dimer at 5, 25, and 65 °C and for the monomer at 25 °C using ensemble-averaged variational transition state theory with multidimensional tunneling (EA-VTST/MT) as previously described.[22,41,54,55] In short, the overall rate constant is calculated from the phenomenological free energy of activation (ΔG_{act}) at temperature T

$$k(T) = \frac{k_B T}{h} \exp[-\Delta G_{act}(T)/RT]$$

where k_B is the Boltzmann constant, h is Planck's constant, and T is the absolute temperature; ΔG_{act} is the sum of the stage-1 quasi-thermodynamic free energy of activation, $\Delta G^{(1)}_{act}$, and a (usually negative) contribution from the transmission coefficient (γ), which contains contributions from dynamical recrossing (Γ) of the barrier and from quantum mechanical tunneling (κ):

$$\Delta G_{act} = \Delta G^{(1)}_{act} - RT \ln \gamma$$

The stage-1 quasi-thermodynamic free energy of activation $\Delta G^{(1)}_{act}$ is obtained by using umbrella sampling to calculate the classical mechanical potential of mean force (CM PMF), $W^{CM}(z)$, where the reaction coordinate z is defined geometrically as the difference between the hydride-donor and the hydride-acceptor distance. The CM free energy of activation is given by the equation

$$\Delta G^{CM}_{act} = W^{CM}(z^*) - W^{CM}(z_R) - G^{CM}_{R,F}$$

where $W^{CM}(z^*)$ is the maximum of $W^{CM}(z)$. The value of $W^{CM}(z_R)$ was set to zero at the reactant state. $G^{CM}_{R,F}$ is the additional CM vibrational free energy of the reactant state that corresponds to mode F, which is normal to the generalized transition state and is not included in the term $W^{CM}(z)$. To obtain $\Delta G^{(1)}_{act}$, the quantized vibration of the nuclei in the predefined primary zone is calculated by instantaneous normal-mode analysis[41] and added to ΔG^{CM}_{act}.

The transmission coefficient γ, which accounts for the dynamical recrossing and the tunneling contribution, was calculated using ensemble-averaged variational transition state theory with a multidimensional tunneling method (EA-VTST/MT). The details of these calculations have been described elsewhere.[55] Briefly, an isoinertial minimum energy path of the primary zone was calculated in the presence of the frozen secondary zone for each configuration. The final transmission coefficient is a value averaged over an equilibrium ensemble of transition state configurations for the secondary zone (14 configurations in the present study).

Minimization and Dynamics. CM-PMF (W^{CM}) was determined using the umbrella sampling technique with a force constant of 150 kcal mol^{-1} $Å^{-2}$ for the harmonic restraint on z. The reaction coordinate z was defined geometrically as the difference between the ($C4_{NADPH}$-H4) and (H4−$C6_{H2F}$) distances. W^{CM} is independent of mass and therefore equally applicable to the unsubstituted and isotopically substituted cases.

The system was gradually heated to the targeted temperature (278.15, 298.15, and 338.15 K) and then equilibrated using an MM method.[22] The average box dimension in the last 10 ps was used in the subsequent QM/MM simulations at constant volume and constant temperature. For the QM/MM simulations, the system was equilibrated for a further 60 ps. Overall, the equilibration stage to prepare the starting structure for the free energy calculations included 90 ps based on the MM potential and 60 ps based on the QM/MM potential. A cutoff distance of 12 Å was used for the nonbonded interactions with a switch function in the region 11−12 Å to feather the interaction energy to zero.

In the calculations of the potential of mean force (PMF), a total of 20 to 22 windows were defined spanning the entire range of the reaction coordinate (z) with a harmonic restraint. The simulations started from the reactant state. Each window was equilibrated for 20 ps and followed by a 40 ps production simulation that collected the probability density of configurations (P) along the reaction coordinate z. Each window was equilibrated for 20 ps and followed by 40 ps of production simulation. During the simulations, the trajectories were saved every 0.1 ps (these saved configurations were used for the covariance analysis described below), and the total simulation time at each temperature was 1200 ps to 1400 ps. The CM-PMF curves were obtained using the weighted histogram analysis method (WHAM).[43,44] After umbrella sampling, the location of the reactant Michaelis state (RS), the transition state (TS), and the product state (PS) were identified. Configurations within 0.1 Å of z (the reaction coordinate) that correspond to RS, TS, and PS were selected to measure the hydrogen bonding distances shown in Table 5.

The subsequent calculations were performed by employing CHARMMRATE,[56] which is based on the interface of CHARMM[57] and POLYRATE.[58] In brief, the quantized vibration correction to the computed classical potential of mean force was obtained from the instantaneous normal-mode analysis of the 31-atom primary zone. 1600 conformations were selected along the umbrella sampling path and used to calculate the quantized vibrational corrections of the isotopically substituted cases.

(53) Casarotto, M. G.; Basran, J.; Badii, R.; Sze, K. H.; Roberts, G. C. K. *Biochemistry* **1999**, *38*, 8038−8044.
(54) Alhambra, C.; Corchado, J.; Sanchez, M. L.; Garcia-Viloca, M.; Gao, J.; Truhlar, D. G. *J. Phys. Chem. B* **2002**, *105*, 11326−11340.
(55) Truhlar, D. G.; Gao, J. L.; Garcia-Viloca, M.; Alhambra, C.; Corchado, J.; Sanchez, M. L.; Poulsen, T. D. *Int. J. Quantum Chem.* **2004**, *100*, 1136−1152.
(56) Garcia-Viloca, M.; Alhambra, C.; Corchado, J.; Sanchez-Ruiz, J. M.; Villa, J.; Gao, J.; Truhlar, D. G. *CHARMMRATE (a module of CHARMM)*, version 2; University of Minnesota, Minneapolis, 2002.
(57) Brooks, B. R.; Bruccoleri, R. E.; Olafson, B. D.; States, D. J.; Swaminathan, S.; Karplus, M. *J. Comput. Chem.* **1983**, *4*, 187−217.
(58) Corchado, J. et al. *POLYRATE 8.5b*. University of Minnesota, Minneapolis, MN, 1999.

In the calculations of the transmission coefficients, the primary zone included 40 atoms. (The specification of which atoms are in the primary zones is provided elsewhere.[22]) The configurations with z within $z^* \pm 0.01$ Å were chosen as the transition state ensemble (TSE). For each configuration of the TS ensemble, the atomic positions of the secondary zone were fixed, and the primary zone atomic coordinates were optimized to the nearest saddle points. Then the isoinertial minimum energy path (MEP) was calculated for this saddle point, and each configuration of the TS ensemble was used to generate a different MEP. As each MEP has a different set of coordinates for the secondary zone, the whole protein and solvent contributed to calculations of the transmission coefficients. The fraction of reaction proceeding by tunneling is actually a lower limit because k includes nonclassical reflection as well as tunneling.

Covariance Analysis. The covariance analysis method uses a collection of configurations of the position of N atoms of the system across the simulation time. Each configuration is translated in space so that the center of the coordinate system is coincident with the center of mass of the structure. Then each configuration is aligned with a reference structure for the approximate removal of overall rotation. The covariance of the spatial atom displacements C_{ij} of atoms i and j is given by

$$C_{ij} = \langle (R_i - \langle R_i \rangle)\,(R_j - \langle R_j \rangle) \rangle$$

where the angle brackets denote the average over the configurations. These covariance elements can then be used to generate the normalized covariance matrix

$$S_{ij} = C_{ij}/(C_{ii}C_{jj})^{1/2}$$

where S_{ij} is an $N \times N$ matrix representing the correlation coefficients of the spatial atom fluctuations between N individual atoms.[59]

For the covariance analysis, the configurations saved in the umbrella sampling along the progression of the reaction coordinate (z) from reactants to products were used to generate the covariance matrices. To test for convergence, only half as many configurations were used and the matrices did not change significantly.

Acknowledgment. We thank the Biotechnology and Biological Sciences Research Council (UK) for financial support (R.K.A.) and Cardiff University for partial funding of a studentship (J.P.). This work was also supported in part by the U.S. National Science Foundation under Grant No. 0349122 and the National Institutes of Health.

Supporting Information Available: Figures S1 and S2 provide matrices of correlated motions of dimeric TmDHFR at 278, 298, and 338 K and RMSDs for QM/MM simulations of the TmDHFR monomer. Complete ref 58. This material is available free of charge via the Internet at http://pubs.acs.org.

JA061585L

(59) Ichiye, T.; Karplus, M. *Proteins* **1991**, *11*, 205−217.